Physics of Fluids

Da Vinci's observation of turbulence: A French-Italian study aiming at numerically reproducing the physics behind one of his drawings, 500 years later

Cite as: Phys. Fluids **33**, 115122 (2021); https://doi.org/10.1063/5.0070984
Submitted: 10 September 2021 • Accepted: 21 October 2021 • Published Online: 16 November 2021

A. Colagrossi, S. Marrone, P. Colagrossi, et al.

Physics of Fluids ARTICLE scitation.org/journal/phf

Da Vinci's observation of turbulence: A French-Italian study aiming at numerically reproducing the physics behind one of his drawings, 500 years later

Cite as: Phys. Fluids **33**, 115122 (2021); doi: 10.1063/5.0070984
Submitted: 10 September 2021 · Accepted: 21 October 2021 ·
Published Online: 16 November 2021

A. Colagrossi,[1,2,a] S. Marrone,[1,b] P. Colagrossi,[3,c] and D. Le Touzé[2,d]

AFFILIATIONS

[1]CNR-INM, Institute of Marine Engineering, 00128 Rome, Italy
[2]ECN/CNRS, École Centrale Nantes, LHEEA Lab., 44300 Nantes, France
[3]Punkt.ink, Roma, Italy

[a]Electronic mail: andrea.colagrossi@cnr.it
[b]Author to whom correspondence should be addressed: salvatore.marrone@cnr.it
[c]Electronic mail: p.colagrossi@punkt.ink
[d]Electronic mail: david.letouze@ec-nantes.fr

ABSTRACT

This research was started in 2019 for the 500th anniversary of Leonardo da Vinci's death. Our Italian-French research group focused its attention on a famous drawing by da Vinci in which a water jet impacts on a pool (RCIN 912660 The Windsor Collection). This particular drawing has often been used by many fluid dynamicists as the first important document concerning turbulent flows. It is worth noting that the word "turbulence," one of the most important phenomena in fluid dynamics, was used for the first time by da Vinci in the "Atlantic codex." After a detailed study of different historical documents, we sought to reproduce the flow drawn in the sheet RCIN 912660 using the Smoothed Particle Hydrodynamics model in order to better analyze the different descriptions that Leonardo reported beside his drawing.

I. INTRODUCTION

Water flows obsessed Leonardo throughout his life (1452–1519). In the years between 1508 and 1511, he studied hydraulics in great detail with the unrealized intention of compiling a treatise on the subject. Leonardo made hundreds of observations on the movement of water and left astute analyses of complex motions in terms of linear and circular components. The superabundance of particular cases and the lack of mathematical tools (it was 300 years before Navier and Stokes) prevented him from ever realizing a set of generally applicable laws.

2019 marked the 500th anniversary of Leonardo da Vinci's death and for this event we planned to present a joint study at the scientific outreach event "La fête de la Science 2019" in Nantes, France. This study started after a 15-year Italian-French collaboration between our two research groups, respectively, the CNR-INM in Italy and the Ecole Centrale Nantes (ECN) in France. Both groups are involved in the study of free-surface flows and develop numerical models for the investigation of such kinds of flow. The main idea was to reproduce one of Leonardo's drawings with in-house solvers developed by the two groups to see if through the analysis of the simulations we would be able to recognize the descriptions written by Leonardo in his notes.

One of the inspirations for this study was the fact that CNR-INM is based in Rome and ECN in Nantes—an ideal prolongation of the path between the cities of Vinci in Italy and Amboise in France, which Leonardo traveled when he was invited by King Francis I of France. He settled in the Manor of Clos-Lucé, which was his residence in the city of Amboise for the last three years of his life.

We started our investigation from the word "turbulence." This phenomenon of paramount importance in fluid dynamics was named for the first time by da Vinci. A famous drawing by Leonardo, reported

in Fig. 1 and labeled as sheet RCIN 912660 of the Windsor collection, depicting a water jet impacting a water pool, has been widely used by fluid dynamicists as an example of a turbulent flow because this drawing is considered to be one of the first attempts to illustrate turbulence (see, e.g., Refs. 14, 26, and 46). Leonardo represented the intrinsic three-dimensional (3D) nature of this turbulent flow with the idea that it consisted of a set of coexisting eddies ranging in scale from large to small. This concept was formalized mathematically 400 years later in 1941 by Kolmogorov and is known as the "cascade model of turbulence."[21]

Figure 2 shows a second drawing by Leonardo. On the right, one can see Leonardo's way of representing a fluid dynamics phenomenon as he saw it or even as he imagined it, with many details of the flow features. The left part of the drawing is a presumed self-portrait of Leonardo observing the phenomenon. Observation and drawing were for Leonardo a true "method of investigation." In fact, historians have shown that by systematically drawing phenomena and parts of the phenomena he was observing, Leonardo was able to analyze these phenomena in detail and even extract rational explanations for them. In this sense, his pictural analysis method was a prelude to the Galilean scientific method, which came about one century later.[32]

In this framework, the present work attempts to address the following questions:

(i) What is the story of the specific drawing shown in Fig. 1?
(ii) What was actually represented by Leonardo (size, conditions, flow characteristics…)?
(iii) How can we reproduce it numerically?
(iv) Is it possible to simulate and visualize all the details da Vinci drew?
(v) Was Leonardo really describing underwater phenomena that he could not even see?

II. METHODOLOGY OF INVESTIGATION

In this section, we describe the global methodology of investigation we pursued. First, we studied the story of da Vinci's hydraulic drawings, of his scientific environment at that time and related analyses in the modern literature. We then focused our attention on the drawing RCIN 912660 in order to determine how specific it is among the body of all his hydraulic drawings. To perform this step, we investigated the story of RCIN 912660 in depth with the help of historians of art and of science, in particular Rodolfo Papa from the Accademia Urbana Delle Arti in Rome and Jean Dhombres from the Centre Alexandre Koyré (EHESS/CNRS) in Paris.

After this investigation, the configuration represented in RCIN 912660 was analyzed in terms of probable ranges of geometrical settings (sizes of the sluice and pool, height of the water jet, depth of the pool, etc.) and of flow conditions (flow rate, incoming level of turbulence, air content in the jet, etc.) with a view of reproducing it numerically as best as possible. To improve this analysis, we also paid attention to the text written under this drawing in which Leonardo describes his understanding of the characteristics of the flow he drew. We thus combined Leonardo's notes with an analysis of the flow characteristics according to our modern physics: intensity of turbulence, characteristics of the vortex scales, complex interaction between air and water, deformation of the free-surface and air bubbles entrapped inside the pool.

Then, in order to plan the simulations, we had to first select the most suitable numerical method to reproduce RCIN 912660. We selected the smoothed particle hydrodynamics (SPH) method with appropriate advanced models among the most recent ones published. Then, we were able to perform preliminary simulations to explore the ranges of geometrical and flow parameters we had previously identified. The influence of air presence was especially investigated.

Once the final configuration had been selected, i.e., that produced the simulations that most resembled Leonardo's drawing, a cutting-edge supercomputer was used to perform detailed simulations involving millions of calculation points. During the post-processing procedure, we used advanced visualization and graphic rendering techniques, to be able to interpret the results of these large simulations. Finally, using our best results, we performed a comparison of the numerical simulations to what was depicted and commented on by Leonardo in his drawing.

III. LEONARDO'S CONCEPT OF TURBULENCE

As stated in the introduction, we started our investigation from the word "turbulence." The first scientific note on turbulence actually dates back to Leonardo da Vinci. He, as well as many of his contemporaries, studied the movement of water in the river courses that were used, at that time, as a means of transport and energy source.

In Fig. 3, the left image depicts an original note by Leonardo on the Codice Atlantico, which reads as follows:

doue la turbolenza dell'acqua si genera
doue la turbolenza dell'acqua si mantiene plugho
doue la turbolenza dell'acqua si posa;

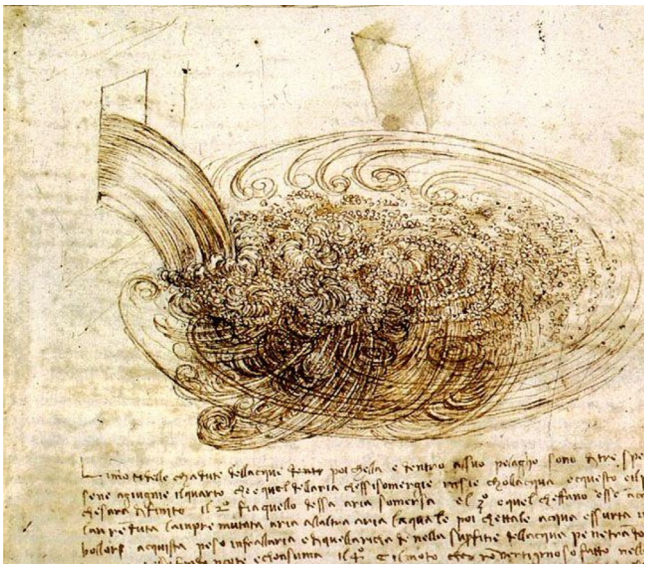

FIG. 1. Leonardo da Vinci's Studies of water (c.1510-12). The fall of a stream of water from a sluice into a pool. Bottom part of the sheet RCIN 912660. Royal Collection Trust Copyright Her Majesty Queen Elizabeth II 2021.

FIG. 2. Presumed to be a self-portrait of Leonardo da Vinci, sketches and notes of wake flows. Sheet RCIN 912579r. Royal Collection Trust Copyright Her Majesty Queen Elizabeth II 2021.

and the corresponding English translation by Macagno[23] is reported on the right. From these and other sentences, we can understand how Leonardo had the novel idea that in many conditions the motion of water is in some way irregular, gives rise to efficient mixing, and possesses a sort of "structure," subject to decay as it moves away from what generated it.

In order to better understand how Leonardo interpreted turbulence phenomena, we followed some of the work performed by Macagno (1914–2012), a Professor at the University of Iowa institute formerly known as the "Iowa Institute of Hydraulic Research" (IIHR). He became an internationally recognized expert on da Vinci's hydraulic studies, and published an extensive series of monographs and articles interpreting the fluid mechanics and flow features of da Vinci's numerous codices and manuscripts. As stated above, we know that "turbulence" in its modern meaning was defined only in 1883 thanks to the experiments of Osborne Reynolds. Therefore, the main question for us was: is the word "turbulence" used by Leonardo really what we mean today by this term? The answer to this question is not straightforward and opinions differ. For example, Macagno wrote the following:

> *We learn for instance (if we know fluid mechanics) that we must be careful in the translation of "turbolenza," because it is certainly not what we call "turbulence" nowadays. I am sure it means instead, "turbidity." It is true that if the sediment is coarse, we must have turbulence for it to be transported, and it is interesting to know that Leonardo knew this; but at this instance, he certainly means "sediment-laden water" and not "turbulent water."*

From this point of view, the main difference between Leonardo's idea of turbulence and the modern meaning is that turbulence is today for us a flow regime and not related to the presence of sediment and to the consequent turbidity of the water. There are various passages in Leonardo's documents where the word "turbulenza" is used, and in which it is always associated with sediment transport, which confirms Macagno's interpretation (see, e.g., Ref. 24).

IV. THE WINDSOR COLLECTION, LEONARDO DA VINCI'S STUDIES OF WATER (C.1510–12)

The previous literature review of da Vinci's view of "turbulence" led us to further investigations of his hydraulic studies/drawings, especially those in the Windsor collection, which contains numerous such studies/drawings of fluid dynamics problems, classified as "Leonardo da Vinci's Studies of water (c.1510–12)."

By the way, it can be noted how peculiar, and lucky in a sense, is the way all these studies by da Vinci came down to us. In the three centuries following Leonardo's death at Amboise, his notebooks were successively dismembered, reassembled into large-format volumes named "Codex," dispersed, sold, lost, taken as spoils of war, lost again, refound, and finally collected, mainly in four places: Milan, Madrid, Windsor, and Paris.

Among the "Studies of water" in the Windsor collection, we focused our attention on sheet RCIN 912660, which contains the drawing that is the subject of our study. In addition to this specific drawing in this collection, there are other works by Leonardo that

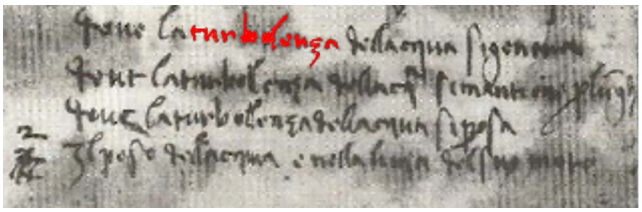

Where the 'turbolenza' of the water is generated.

Where the 'turbolenza' of the water persists for a long distance.

2. Where the 'turbolenza' of the water settles.

FIG. 3. Left: Leonardo's original note on the Codice Atlantico, CA 201 V (74 v.a + 74 v.b) c. 1505-6 (inverted horizontally because of Leonardo's direction of writing from right to left), first column where the word "turbulence" (highlighted in red) is used in a fluid dynamics context. Right: Translation of the note on the left by Macagno (University of Iowa).[23]

played a relevant role in our investigation. Some of them are reported and briefly commented on in this section.

The sheet RCIN 912660 is composed of two parts. In the upper part, there are drawings of flow past a free-surface piercing plate as reported in the picture on the left in Fig. 4. In this drawing, Leonardo reproduced the complex motion of the free surface in a detailed way, highlighting some flow features, such as the generation of vortical structures linked to breaking wave phenomena. As many scholars have remarked, the surface motion resembles curly hair as in his drawing representing the "Head of Leda" (sheet RCIN 912518, see right-hand part of Fig. 4). Leonardo observed the motion of the water surface and identified two components: one which follows the main current, while the other forms the lines of the eddies.

This decomposition can be linked to the modern meaning of the term "turbulent flow" coined much later in 1883 thanks to the experiments of Osborne Reynolds.[20,36] In Reynolds' work, the transition from laminar to turbulent flow is identified thanks to the dimensionless number that bears his name and represents the ratio between inertial and viscous forces. Once a turbulent flow regime is established, the velocity field can be decomposed into two parts: one represents a time averaged component and the other contains the high frequency chaotic fluctuations. The latter are related to the action of turbulent eddies. It is worth noting that in his paper,[36] Osborne Reynolds represented the turbulent flows observed in his experimental apparatus by means of drawings, using Leonardo's approach (see Fig. 5). In this article, Reynolds made the following comment on this sketch: "On viewing the tube by the light of an electric spark, the mass of colour resolved itself into a mass of more or less distinct curls, showing eddies."

The bottom part of the sheet RCIN 912660 contains the drawing that is the subject of the present work (picture on the left in Fig. 6): the fall of a stream of water from a sluice into a pool in which the multiple layered vortices are seen extending far below the surface, and where entrapment of air and the subsequent upward movement of air bubbles is also evident. From this drawing and the notes reported alongside, it is clear that Leonardo focused his attention on the air–water interactions, as he wrote,

> *"the beautiful movements which result from one element [air] penetrating another [water]."*

This drawing exemplifies da Vinci's ability to fix on paper all the features of a complex unsteady flow motion that he observed.

FIG. 4. Left: Leonardo's drawing of the flow past a pierced inclined plate. Upper part of the sheet RCIN 912660. Right: The Head of Leda (c.1505-08) (sheet RCIN 912518). Royal Collection Trust Copyright Her Majesty Queen Elizabeth II 2021.

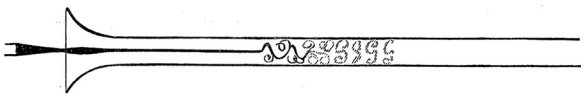

FIG. 5. Reynolds' sketch showing the loss of the laminar regime observed through his experimental apparatus. The thin ink line transported by the fluid rightward abruptly changes, forming more or less distinct curls.[36]

In recent studies, reported in the book,[12] thanks to the use of a range of noninvasive techniques, including ultraviolet imaging, infrared reflectography, and x-ray fluorescence, it was possible to see the under-drawing of the sheet RCIN 912660 (see picture on the right in Fig. 6). The latter is much simpler than the final pen drawing, which is a dense layering of water currents and bubbles (left-hand drawing in Fig. 6). Thanks to this analysis, it can now be understood how Leonardo built up his final picture in stages: he started with an underlying structure of currents in sweeping whorls, and then added the little rosettes of bubbles on the surface and, more generally, all the surface details.[7] It is worth also recalling that Leonardo was fascinated by the motion of rising bubbles in still water, a phenomenon that is nowadays commonly known as Leonardo's paradox (see Ref. 26).

The text Leonardo wrote below his drawing describes the details of the five main air–water flow features he identified:

1. the air submerging with the water;
2. the motion of the submerged air, which rises in the shape of large bubbles;
3. the upward movement produced by the water transported with the rising air bubbles when they ascend back to the surface of the water;
4. the downward movement produced by the water jet that continues its way toward the bottom that it strikes and consumes; and
5. the large eddy movements made on the surface of the pool by the water that flows back to the jet impingement location, the latter being the lowest place of the disturbed pool surface.

In a last block of text, da Vinci finally wrote,

"But the part of impetuous water which is between the air and the other water cannot respond for long to the said impetus on account of its weight, which deprives it of the quickness and fluency of its motion, and therefore does not go through a complete circumvolution."

This last sentence shows that Leonardo observed that the impinging water, made of underwater eddies, rapidly lost its momentum ("quickness and fluency of motion"), which he intuited was linked to its high, non-buoyant density ("weight"). To some extent, he was thus intuiting that there is a turbulent kinetic energy decay in space and time, especially in zones of intense vorticity.

The above analysis identifying the main air–water flow features can be better assessed by looking at other sheets in the "Studies of water" collection. Figure 7 shows two different drawings presented in the sheet RCIN 912662. From these drawings, it is clear that Leonardo focused his attention on the vortex structures formed by the impinging water jet, vortices which develop and are advected by the flow current inside the bulk of the fluid. In these drawings, the dynamics of the entrapped air is completely absent. Conversely, in Fig. 8 only the air bubbles reaching the pool surface are reported. This is further proof that Leonardo was categorizing the different flow features, drawing them separately as in the sheet RCIN 912662 or combining them in a more complex and complete view as in the sheet RCIN 912660.

The flow features observed by da Vinci in the sheet RCIN 912660 have been highlighted so far. A numerical simulation able to replicate in detail those observations would make it possible to verify how accurately the painter was able to describe the physical reality involving phenomena even when not clearly visible, and to what extent his understanding of the different flow features corresponds to their scientific description today. It would also make it possible to discuss in modern terms this kind of phenomena. In particular, it would be possible to evaluate the importance of the turbulent structures developed by the shear layers generated by the falling water jet inside the water pool, with respect to that of the turbulence generated by the motion of entrapped air that rises up toward the pool surface in the form of a bubble cloud. Another aspect that remains unclear from the drawing examined and on which a numerical simulation could shed some light is how the water pool surface is affected by the above two sources of turbulence and how intense the surface eddies and the gravity waves generated by it are.

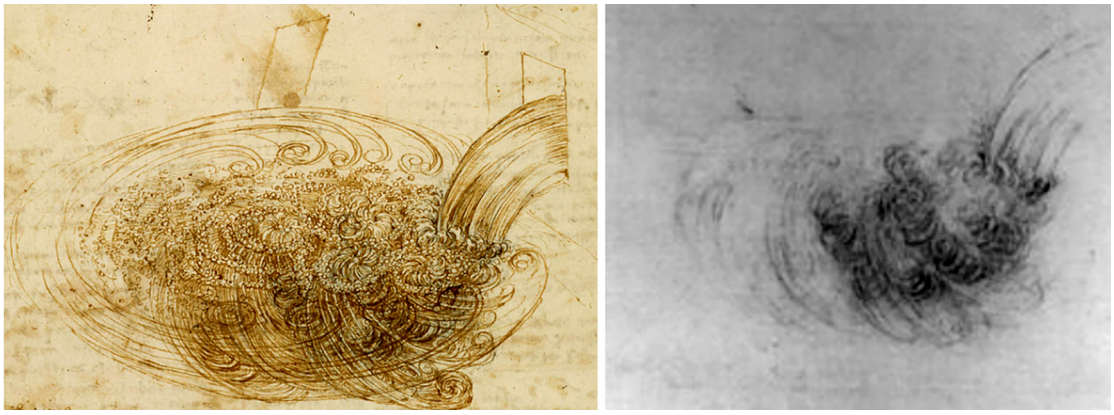

FIG. 6. Left: Studies of water (c.1510-12). Sheet RCIN 912660. Right: The under-drawing shown under infrared light.[12] Royal Collection Trust Copyright Her Majesty Queen Elizabeth II 2021.

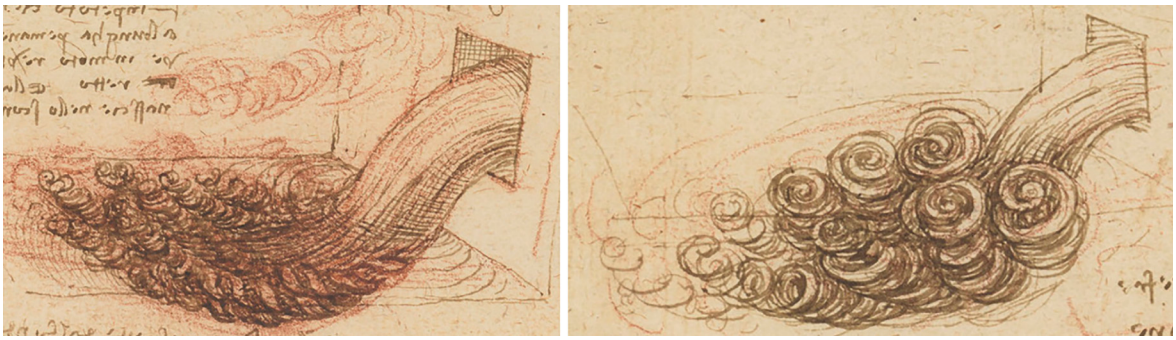

FIG. 7. Studies of water (c.1510-12). Two details at the bottom of the sheet RCIN 912662. Royal Collection Trust Copyright Her Majesty Queen Elizabeth II 2021.

V. CHALLENGES IN MEASURING AIR–WATER TURBULENT FLOWS USING MODERN EXPERIMENTAL SETUPS

Looking at the flow reproduced by Leonardo in the sheet RCIN 912660, before reproducing this kind of flow through a numerical code, one could consider an experimental study. However, even nowadays the experimental approach presents several challenges in measuring an air–water turbulent flow. Modern experimental setups are based on the use of optical techniques such as LDV (laser Doppler velocimetry)[13] or PIV (particle image velocimetry)[1] due to their non-intrusive nature and to their higher accuracy compared to traditional velocimetry techniques such as, e.g., Pitot tube and hot wire. In particular, over the past two decades, PIV-based techniques have matured considerably and have been finding broadening use in fluid mechanics research. PIV and its variants (stereo-PIV, tomographic PIV) are whole-field instantaneous measurement techniques that yield either two or three velocity components in a single plane or in a volume. This characteristic along with the availability of increasingly powerful hardware components, such as high-energy pulse lasers and high-resolution and low-noise charged-coupled device (CCD) cameras, have made these techniques uniquely suitable for the investigation of complex non-linear flow phenomena, involving large unsteady flow structures, as in the case of wake flows behind a rotating propeller (see, e.g., Refs. 15 and 16).

In recent years, PIV has also been applied to the study of multi-phase flows. However, its application there is very challenging, particularly due to the presence of phase interfaces that block the optical path to the measurement location in bubbly flows, thus affecting both the penetration of the illuminating light and the light along the optical path to the recording medium. More specifically, PIV is only practicable at low fractions of solid particles or gas bubbles of values less than about 5%.[5] It follows that velocity measurements in high void fraction bubbly flows, as in the case of the water flow pouring into a pool of the sheet RCIN 912660, still remain arduous to address experimentally.

FIG. 8. Studies of water (c.1510-12). Details at the top of the sheet RCIN 912662. Royal Collection Trust Copyright Her Majesty Queen Elizabeth II 2021.

In order to overcome these difficulties, some promising techniques have been developed, for example measuring fluid shear stress using the cell flashing behavior of bioluminescent dinoflagellates. In Refs. 9 and 40, this technique was used to estimate a heterogeneous time-varying shear stress inside a breaking wave crest. This technique was further developed in Ref. 10 to study the turbulent flow generated by a rising bubbly flow. In that work, it was shown how the bioluminescence of the dinoflagellate *Lingulodinium polyedrum* is influenced by the size of the air bubbles.

VI. NUMERICAL SIMULATION AIMING AT REPRODUCING AT BEST THE FLOW CONDITION DRAWN IN THE SHEET RCIN 912660

A. The smoothed particle hydrodynamics method and the multi-phase δ-LES-SPH model adopted

The SPH method was developed in the seventies for studying astrophysical flows such as those involved in star formation.[17,22] This method is still used nowadays to simulate the evolution and assembly of galaxies (see, e.g., Ref. 37). In the 1990s, the method was extended to free-surface flows by Monaghan[27] who also performed a first attempt to reproduce the drawing RCIN 912660 using the SPH method in the work by Monaghan and Kajtar.[29] The latter study was performed in a two-dimensional (2D) framework without taking into account the presence of air. Under these too restrictive simplified conditions, the dynamics of the flow is very different to what was described by Leonardo. On the other hand, this article showed the capability of this numerical method to simulate turbulent flows where an air–water interface is present, therefore inspiring the present study. Among the different variants of SPH developed in recent decades, we selected the δ-LES-SPH model described in Ref. 11 and recently further extended in Ref. 3. In the present work, this δ-LES-SPH model was adapted to the multi-phase flow context following the work of Hammani *et al.*,[19] in which the pressure field is linked to the density field through the use of a stiff equation of state as follows:

$$p_i = f_\chi(\rho_i) = \frac{\rho_{0\chi} c_{0\chi}^2}{\gamma_\chi}\left[\left(\frac{\rho_i}{\rho_{0\chi}}\right)^{\gamma_\chi} - 1\right], \quad \forall\, i \in \chi, \tag{1}$$

where γ_χ is the polytropic coefficient of phase χ and $c_{0\chi}$ is its speed of sound (χ being air or water in the present work). It is worth stressing that the equation of state in Eq. (1) is adopted for both air and water phases, as they are both treated as weakly compressible media. Regarding the speed of sound, the procedure to select suitable values can be found in Ref. 19.

In the following, the δ-LES-SPH model is briefly recalled. For the sake of brevity, only the most relevant information is reported, and the interested reader is referred to the cited articles for further details. The governing equations are the Navier–Stokes equations written in an arbitrary-Lagrangian–Eulerian (ALE) framework, which are discretized within the SPH context as follows (for details, see Ref. 3):

$$\begin{cases} \dfrac{\mathrm{d}\rho_i}{\mathrm{d}t} = -\rho_i \displaystyle\sum_j (\boldsymbol{u}_{ji} + \delta\boldsymbol{u}_{ji}) \cdot \nabla_i W_{ij}\, V_j + \mathcal{D}_i^\rho \\ \qquad\qquad + \displaystyle\sum_{j\in\chi} (\rho_j\, \delta\boldsymbol{u}_j + \rho_i\, \delta\boldsymbol{u}_i) \cdot \nabla_i W_{ij}\, V_j\,, \\ \rho_i \dfrac{\mathrm{d}\boldsymbol{u}_i}{\mathrm{d}t} = \boldsymbol{F}_i^p + \boldsymbol{F}_i^v + \boldsymbol{F}_i^{st} + \rho_i \boldsymbol{g} \\ \qquad\qquad + \displaystyle\sum_{j\in\chi} (\rho_j\, \boldsymbol{u}_j \otimes \delta\boldsymbol{u}_j + \rho_i\, \boldsymbol{u}_i \otimes \delta\boldsymbol{u}_i) \cdot \nabla_i W_{ij}\, V_j\,, \\ \dfrac{\mathrm{d}\boldsymbol{r}_i}{\mathrm{d}t} = \boldsymbol{u}_i + \delta\boldsymbol{u}_i\,, \quad V_i = m_i/\rho_i\,, \quad p_i = f_\chi(\rho_i)\,, \quad \forall i \in \chi, \end{cases} \tag{2}$$

where the subscripts i and j refer to the generic i-th and j-th particles; $\boldsymbol{F}_i^p$, $\boldsymbol{F}_i^v$, and $\boldsymbol{F}_i^{st}$ are the pressure, viscous and surface tension forces, respectively, acting on particle i. The vector field $\delta\boldsymbol{u}$ is the particle shifting velocity adopted to regularize the particles' spatial distribution during their motion. The notation $\boldsymbol{u}_{ji}$ indicates the difference $(\boldsymbol{u}_j - \boldsymbol{u}_i)$ and the same holds for $\delta\boldsymbol{u}_{ji}$ and $\boldsymbol{r}_{ji}$. χ denotes the phase of particle i; summations for $j \in \chi_i$ are thus computed only using particles belonging to the same phase.

The particle masses m_i are assumed to be constant during their motion. The particles are set initially on a Cartesian lattice with spacing Δr, and hence, the particle volumes V_i are evaluated initially as Δr^n (where n is the number of spatial dimensions) and the particle masses m_i are then calculated through the initial density field (using the equation of state and the initial pressure field). During the time evolution, volumes V_i change accordingly with particle densities ρ_i. The spatial gradients are approximated through convolution summation with a kernel function W_{ij}. As in Ref. 3, a C2-Wendland kernel is adopted in the present work.

The time derivative d/dt used in Eq. (2) indicates a quasi-Lagrangian derivative, i.e.,

$$\frac{d(\bullet)}{dt} := \frac{\partial(\bullet)}{\partial t} + \nabla(\bullet) \cdot (\boldsymbol{u} + \delta\boldsymbol{u}),$$

since the particles are moving with the modified velocity $(\boldsymbol{u} + \delta\boldsymbol{u})$ and the above equations are written in an arbitrary-Lagrangian–Eulerian framework. For this reason, the continuity and the momentum equations contain terms with spatial derivatives of $\delta\boldsymbol{u}$ (for details see Ref. 3).

The term $\mathcal{D}_i^\rho$ is the numerical diffusive term introduced by Ref. 2 to filter out the spurious high-frequency noise in the pressure field. Following Ref. 3, this term is rewritten within an Large Eddy Simulation (LES) framework as follows:

$$\begin{cases} \mathcal{D}_i^\rho := \sum_{j\in\chi}\, \delta_{ij}\, \boldsymbol{\psi}_{ji} \cdot \nabla_i W_{ij}\, V_j\,, \\ \boldsymbol{\psi}_{ji} := 2\left[(\rho_j - \rho_i) - \dfrac{1}{2}\left(\langle\nabla\rho\rangle_i^L + \langle\nabla\rho\rangle_j^L\right)\cdot \boldsymbol{r}_{ji}\right]\dfrac{\boldsymbol{r}_{ji}}{||\boldsymbol{r}_{ji}||^2}, \\ \delta_{ij} := 2\,\dfrac{\nu_i^\delta\, \nu_j^\delta}{\nu_i^\delta + \nu_j^\delta}\,, \quad \nu_i^\delta := (C_\delta\, l)^2\, ||\mathbb{D}_i||. \end{cases} \tag{3}$$

In the first equation, since the summation is based on the χ phase the density diffusion is blocked across the air–water interface. The constant C_δ is a dimensionless constant set equal to 6 while $l = 3\Delta r$ is the radius of the kernel W support and represents the length scale of the filter adopted for the sub-grid model. The tensor $\mathbb{D}$ is the symmetric part of the velocity gradient and $||\mathbb{D}||$ is a rescaled Frobenius norm, i.e., $||\mathbb{D}|| = \sqrt{2\mathbb{D} : \mathbb{D}}$. The superscript L in Eq. (3) indicates that the gradient is evaluated using the renormalized gradient, i.e.,

$$\begin{aligned} \langle\nabla\rho\rangle_i^L &= \sum_j (\rho_j - \rho_i)\, \mathbb{L}_i^{-1}\, \nabla_i\, W_{ij}\, V_j\,, \\ \mathbb{L}_i &:= \left[\sum_k (\boldsymbol{r}_j - \boldsymbol{r}_k) \otimes \nabla_i\, W_{ik}\, V_k\right], \end{aligned} \tag{4}$$

where $\mathbb{L}_i$ is the renormalization matrix (see, e.g., Ref. 35).

The viscous forces $\boldsymbol{F}^v$ are expressed as follows:

$$\begin{cases} \boldsymbol{F}_i^v := 2(n+2) \displaystyle\sum_j (\mu_{ij} + \mu_{ij}^T)\, \pi_{ij}\, \nabla_i W_{ij}\, V_j\,, \\ \mu_{ij} := 2\,\dfrac{\mu_i\, \mu_j}{\mu_i + \mu_j}\,, \quad \pi_{ij} := \dfrac{\boldsymbol{u}_{ij}\cdot\boldsymbol{r}_{ij}}{||\boldsymbol{r}_{ji}||^2}\,, \\ \mu_{ij}^T := 2\,\dfrac{\mu_i^T\, \mu_j^T}{\mu_i^T + \mu_j^T}\,, \quad \mu_i^T := \rho_0\, (C_S\, l)^2\, ||\mathbb{D}_i||, \end{cases} \tag{5}$$

where μ is the dynamic viscosity of the specific phase related to the particle i or j. This viscous term contains both the effect of the latter real viscosity μ and of the one related to the local turbulent viscosity μ^T, which is modeled through a simple Smagorinsky model where the constant C_S is set equal to 0.18 (see Ref. 39).

The pressure forces $\boldsymbol{F}_i^p$ are expressed as follows:

$$\begin{cases} \boldsymbol{F}_i^p = -\displaystyle\sum_i (p_j + p_i)\, \nabla_i\, W_{ij}\, V_j + S_i \sum_j \nabla_i\, W_{ij}\, V_j, \\ S_i = \begin{cases} 0, & p_i \geq 0, \\ 2p_i, & p_i < 0, \quad i \notin \mathcal{S}_F, \end{cases} \end{cases} \tag{6}$$

where $\mathcal{S}_F$ denotes the region of the fluid domain close to the free surface, that is the free-surface particles and their neighboring particles. The free-surface particles are detected through the algorithm described in Ref. 25. Equation (6) corresponds to a switch from the "plus" formulation (namely, $p_j + p_i$) to the "minus" formulation (that is, $p_j - p_i$) when the pressure p_i is negative inside the fluid region. This switch removes the so-called "tensile instability,"[44] which is a numerical instability of the SPH scheme. As remarked in Sun *et al.*[41] especially for high Reynolds number regimes, tensile instability can induce numerical cavitation in the cores of the eddies caused by the pressure drops inside these flow regions. Furthermore, when the occurrence of

numerical cavitation is prevented by the action of shifting velocity $\delta \boldsymbol{u}$ alone, without using Eq. (6), it can alter the vorticity field by adding numerical noise.

Then, similar to what was already underlined by Grenier *et al.*,[18] when using the models presented above to simulate multi-phase flows where surface tension effects are negligible, a nonphysical interpenetration of particles belonging to different phases may occur, leading to a numerical fragmentation of the fluid interfaces. In order to prevent this, a small repulsive force was introduced to mimic a surface tension force as follows:

$$\boldsymbol{F}_i^{st} = \epsilon_\chi \sum_{j \in \bar{\chi}} \left(|p_i| + |p_j| \right) \nabla W_{ij} \, V_j, \tag{7}$$

where ϵ_χ is a parameter in the range $[0.01 - 0.1]$. In the present work, $\epsilon_\chi = 0.01$ is adopted. The summation applies to particles that do not belong to the same fluid as that of the i-th particle; this set of particles is noted by $\bar{\chi}$. As shown in Ref. 8, Eq. (7) models a cohesion force, i.e., a surface tension, as also explained in Ref. 30. In Szewc *et al.*,[45] it is shown in a heuristic way how the spurious interface fragmentation in multi-phase SPH can be controlled by the coefficient ϵ_χ.

Finally, the particle shifting velocity $\delta \boldsymbol{u}$ is given by

$$\begin{cases} \delta \boldsymbol{u}_i^* = -0.1 \, l \, c_{0\chi} \sum_j \left[1 + R \left(\dfrac{W_{ij}}{W(\Delta r)} \right)^n \right] \nabla_i W_{ij} V_j \, , \\ \delta \boldsymbol{u}_i = \min \left(||\delta \boldsymbol{u}_i^*||, \dfrac{\max_j ||\boldsymbol{u}_{ij}||}{2} \right) \dfrac{\delta \boldsymbol{u}_i^*}{||\delta \boldsymbol{u}_i^*||} \, . \end{cases} \tag{8}$$

Here, the constants R and n are, respectively, set to 0.2 and 4 as in Refs. 28 and 42. Following Ref. 42, particle shifting is allowed only in the tangential directions for particles close to the air–water interfaces. The second equation of Eq. (8) is introduced to limit the magnitude of shifting velocity for the purpose of robustness. Since Eq. (8) is proportional to the smoothing length, the intensity of $\delta \boldsymbol{u}$ decreases as the spatial resolution increases, and this guarantees that $\delta \boldsymbol{u}_i$ induces small deviations with respect to the physical particle trajectory. As documented in Ref. 42, the use of the particle shifting technique (PST) leads to regular particle distributions and increases the accuracy and the robustness of the scheme. In turn, the inclusion of the PST causes the loss of exact conservation of angular momentum as discussed in Refs. 4 and 42. It is worth noting that the shifting velocity close to the air– water interface has to be modified to be consistent with the kinematic boundary condition along such an interface. In particular, the normal component of $\delta \boldsymbol{u}$ to this interface has to be nullified while the tangential component is maintained unaltered (for more details, see Ref. 42).

B. Simulation setup

As mentioned above, the first problem in numerically reproducing the flow drawn by Leonardo Da Vinci in the sheet RCIN 912660 is the fact that we have no information about the geometry and the flow conditions.

Therefore, we started by performing preliminary tests in order to set the simulation parameters in terms of the following:

- Determination of the problem geometry:
  - jet dimension and height above the pool,
  - pool size,
  - walls and outlet configuration, and
  - inlet conditions.
- Identification of numerical parameters and CPU requirement, i.e., the parameters linked to the SPH model presented in Sec. VI A: particle size, etc.
- Study of the relevance of air entrainment and the effect of the percentage of air/water mixture at inlet.
- Detection and visualization of the vortex structures (Q-criterion, vorticity modulus, finite time Lyapunov exponent).

On the basis of the limits encountered in the previous study in Ref. 29, all the simulations of the present study, including those of this preliminary stage of the work, were performed in the 3D framework.

C. Single-phase simulations

Two series of very preliminary tests were first performed, which are briefly reported here to show our approach, but without reporting all the details. In these first test cases, the water jet was generated by an inlet boundary that fills a small chamber positioned above the pool. The water overflows the small chamber and falls into the pool below which is partially filled with calm water.

Snapshots of a 2D slice for the first two tests we ran are reported in Fig. 9. In the left plot of Fig. 9, a shallow pool was used. The shear layers generated by friction between the impinging jet and the still water are clearly visible from the vorticity field. These shear layers are then deflected by the bottom and the lateral walls. In the right plot of the same figure, a deeper pool is used. In this case, the previous shear layers become unstable and a turbulent flow is generated, forming small eddies. The deflection of vortical structures by the bottom and lateral walls is still clearly visible. As expected, the water pool surface is less disturbed in the deeper pool than in the shallower pool case.

From those plots, it is also possible to see that the water can exit by overtopping the lateral walls. For the second test case (deeper pool, right plot), the height of the left wall was slightly lower so that the water exited from this side of the domain avoiding a rightward water exit from the pool, which could disturb the falling jet (see left plot). The flow exiting from the lateral wall(s) induces the establishment of a current, which also transports the vortical structures. The vorticity in this configuration is therefore confined in the region close to the walls, in addition to the plunging jet itself.

In a second series of tests, the configuration was slightly modified. The simulations started with a half-empty water pool so that turbulence structures had more time to spread in the domain and to interact with the pool surface. The left plot of Fig. 10 shows half of the domain, with particles colored by the modulus of the vorticity field, at the time when the water has reached its maximum height. The vortex structures are again concentrated close to the solid boundaries; however, this time they reach the water surface and strongly interact with it: whirlpool formations are clearly visible on the liquid surface. The right plot of Fig. 10 reports the same time instant; here, the particles on the pool surface are colored with their vertical position and the 3D view has been changed in order to better highlight the depressions (low elevation) of the free surface in correspondence with the center of the vortices.

So far, the results of the first two series of preliminary simulations remain quite far from what Leonardo drew and commented on in

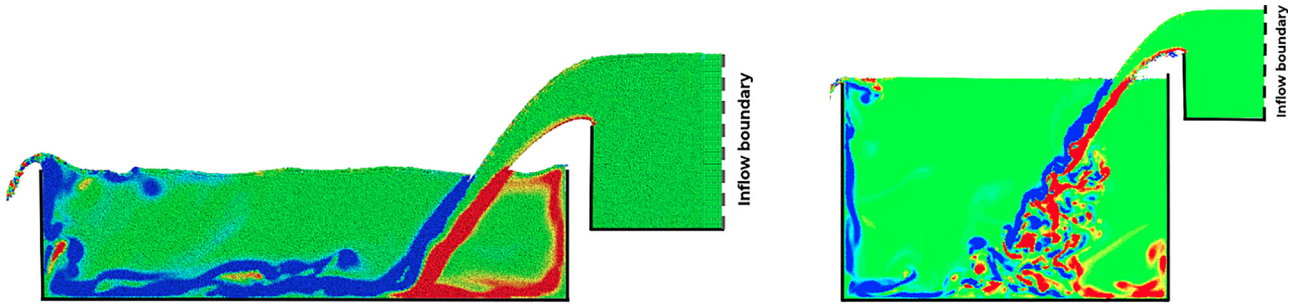

FIG. 9. Preliminary SPH tests using a single-phase model (air phase is not included)—first series. Slice of the fluid domain in the z–x mid-plane. Left: shallow water pool. Right: deep water pool. Colors are representative of the component of the vorticity field orthogonal to the plotted slice of the 3D simulation (red anticlockwise, blue clockwise).

terms of flow features. Therefore, further configurations needed to be tested.

In particular, from Figs. 9 and 10 one can see that the water jet formed in the chosen configuration, using two water containers at different heights (the chamber and the pool), tends to expand in the $y-$ direction during its fall and, consequently, to become thinner when approaching the water pool. For this reason, all the further simulations were performed by generating the water jet directly using an inlet boundary over the pool without using a preliminary chamber.

This modification was the subject of a third series of tests. Figure 11 reports two plots extracted from those tests. The left plot refers to a test with a low particle resolution, $H_J/\Delta r = 25$, where H_J is the size of the considered-square jet at the inflow boundary. The inflow velocity was set as $U = 1.5$ m/s, $H_J = 0.4$ m. The pool is initially completely filled with water so that the initial water height in the pool is $H_W = 3.5\,H_J$ and is equal to the height of the vertical walls. The inflow elevation from the water surface is $H_I = 1.38\,H_J$. The jet is generated at the inlet at the initial time $t = 0$. In the left plot of Fig. 11, the sketch of the problem geometry adopted is reported. The bottom of the pool has a square shape with side $L_p = 7.5\,H_J$. The inflow velocity was prescribed through a velocity profile mimicking the boundary layer effects of a (possibly present) sluice gate as reported in the inset of Fig. 11. This velocity profile was applied both in the x- and z-directions of the inlet.

The Froude number was defined as $\mathrm{Fr} = U/\sqrt{g\,H_J} = 0.757$ while the Reynolds number was set equal to $\mathrm{Re} = \rho U H_J/\mu = 600\,000$ by adopting the water density and dynamic viscosity. In the right plot of Fig. 11, a slice of the vorticity field obtained through a large eddy simulation is reported. As a consequence of the velocity profile at the inlet, the vorticity field inside the jet is not uniform and its free surface presents irregularities linked to the flow instability. The latter induces a quicker inception of the instability of the shear layers developed in the pool where an intense turbulent flow is established. For this test case, the resolution was increased up to $H_J/\Delta r = 60$.

The simulation lasted 10.4 s of physical time and involved, on average, about 50 million particles for 37 000 time iterations. The simulation ran for 102 h on 360 cores of the "Liger" supercomputer at Ecole Centrale de Nantes equipped with 12-core Intel Xeon (Haswell) E5–2680v3 processors.

From the results presented in the right plot of Fig. 11, one can see that the underwater water jet appears more similar to what Leonardo drew. In particular, the large vortical structures formed in the front part of the underwater jet correspond well to what was discussed in Fig. 6 where the underlying underwater vortical structures drawn by

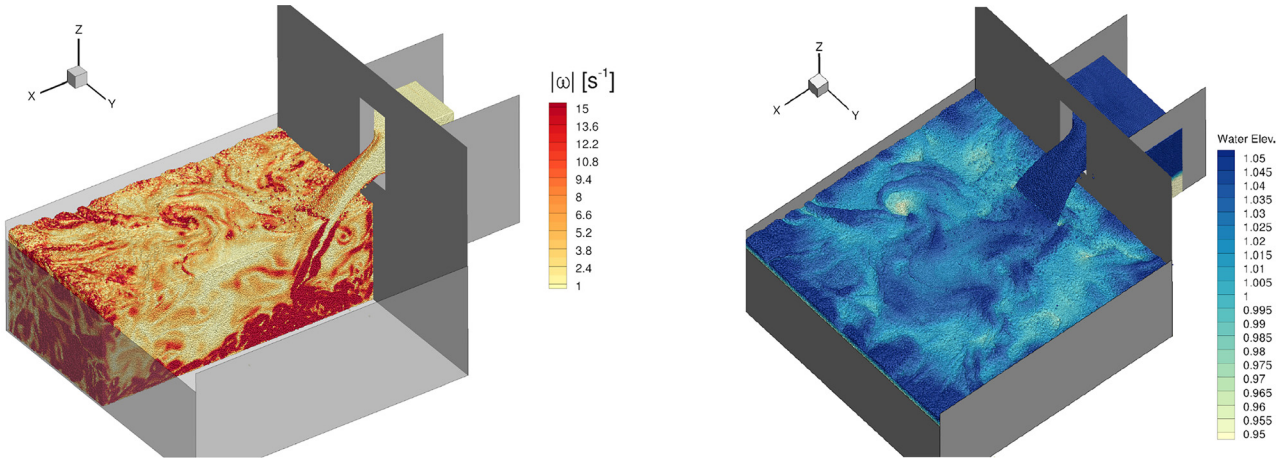

FIG. 10. Preliminary SPH tests using a single-phase model—second series. Left: Visualization of the particles in half-domain. The colors are representative of the modulus of the vorticity field. Right: top view of the particles at the water surface, which are colored using their vertical position.

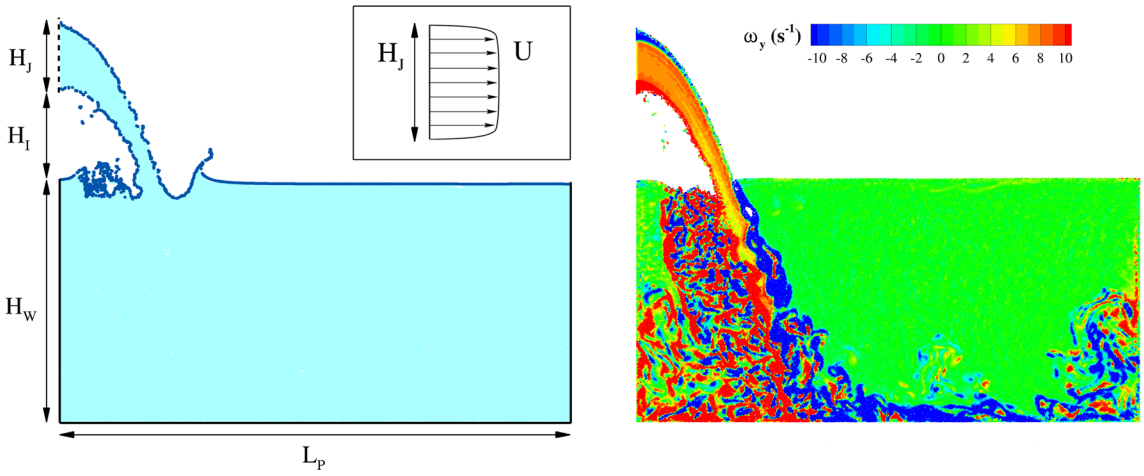

FIG. 11. Preliminary SPH tests using a single-phase model—third series. Left: sketch of the 2D mid-section of the geometrical configuration adopted for the third test case series. Right: slice of the fluid domain in the *z*–*x* mid-plane at time 5.0 s for Reynolds number Re = 600 000. Colors are representative of the y-component of the vorticity field (red clockwise, blue anticlockwise).

da Vinci were evidenced. From this observation and the already quite high CPU cost of this Re = 600 000 simulation, we decided to keep it as our final study configuration (except for the presence of air, which will be studied in Sec. VI D).

The left plot of Fig. 12 shows a 3D view of the water jet and of the water pool surface. A slice of the flow domain is also reported with the particles colored with the *y*-vorticity. In the right plot, the mid *z*–*x* plane is colored with the modulus of velocity. The maximum speed reached is about 4 m/s. From this contour plot, the turbulent regime of the flow field can be clearly observed. The turbulent energy is mainly focused close to the shear layers while the rest of the domain remains almost at rest.

A contour plot of the turbulent viscosity, μ_T, in the mid *z*–*x* plane at time 5.0 s is depicted on the left plot of Fig. 13. In correspondence of the most intense vortical structure, the ratio μ_T/μ reaches a value of about 100, indicating that the spatial resolution adopted is still insufficient to resolve all the scales of the inertial range.[33] The right plot of the same figure shows the contour plot of the finite time Lyapunov exponent (FTLE). In Ref. 43, it was shown how this quantity can identify Lagrangian coherent structures much better than quantities derived from the velocity gradient. However, the latter technique seems to provide satisfactory results only for direct numerical simulations, where all the vortical scales are resolved and FTLE can be evaluated with sufficient detail. Conversely, in our large eddy simulations the details of the FTLE were too poor to identify the vortical structures: as shown in the right plot of Fig. 13 for $\lambda > 4\ s^{-1}$, the details of the vortical structures start to be lost.

In order to represent the vortical structures in their 3D shape, post-processing of the SPH data is needed. For this procedure, a subset of the particles was identified using the modulus of vorticity field.

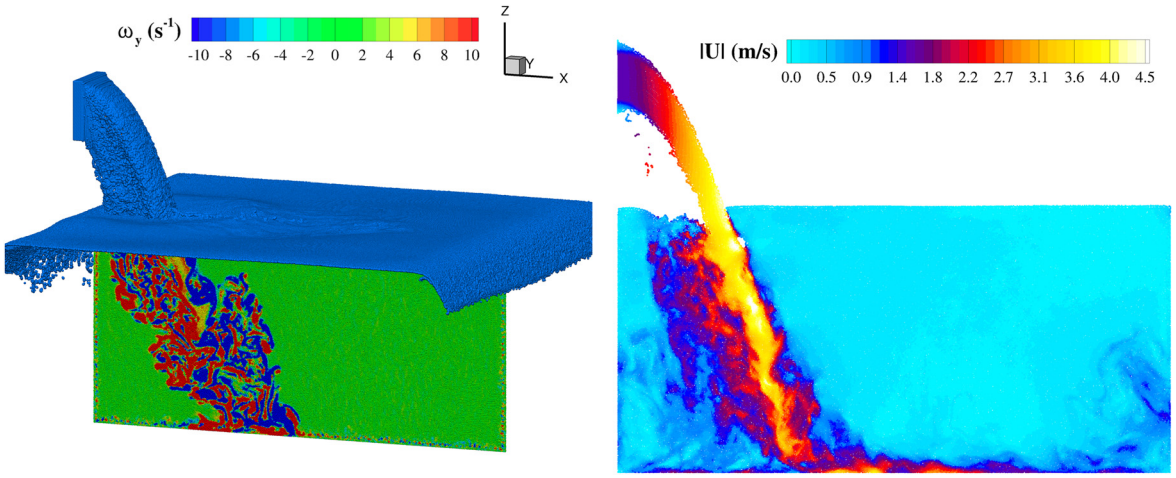

FIG. 12. SPH simulation using a single-phase model (air phase is not included)—final configuration. Left: 3D view of the free surface with two slices of the domain where particles are colored with the *y*-vorticity component at time 1.5 s. Right: contour plot of the modulus of the velocity in the mid *z*–*x* plane at time 5.0 s.

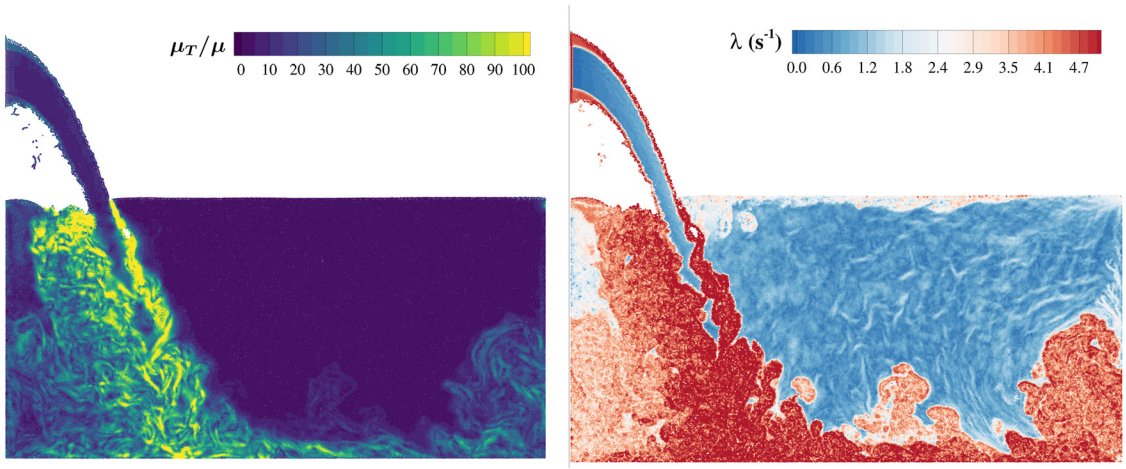

FIG. 13. SPH simulation using a single-phase model (air phase is not included)—final configuration. Left: contour plot of the turbulent viscosity in the mid *z*–*x* plane at time 5.0 s. Right: contour plot of the FTLE in the mid *z*–*x* plane at time 5.0 s.

An example is given in the left plot of Fig. 14 where only the particles having $|\boldsymbol{\omega}| < 30\ \mathrm{s}^{-1}$ are selected and plotted. From this particle subset, a surface can be constructed by interpolating and approximating surfaces from a polygon soup algorithm (see, e.g., Ref. 38). Once the surface has been extracted, a rendering procedure is executed. The right plot of Fig. 14 depicts such a rendering of an iso-surface of $|\boldsymbol{\omega}|$. This rendering procedure highlights the different scales of vortices from the largest ones related to the shear layers up to the smaller secondary vortical structures concentrated close to the pool walls.

The vortical structures can also be identified with the use of the Q-criterion calculated as follows:

$$Q = \frac{\mathbb{W}^2 - \mathbb{D}^2}{2}, \tag{9}$$

where $\mathbb{W}$ is the anti-symmetric part of the velocity gradient tensor. To capture the vorticity structures, only the particles having a Q value greater than a certain positive threshold are selected. The vortical structures are better identified compared to the use of $|\boldsymbol{\omega}|$ so that we decided to use iso-Q renderings to proceed with the analysis. Figure 15 shows an iso-Q surface that is colored with the intensity of the velocity field to improve the rendering. In the figure, the main lengths of the problem are also reported.

Finally, in the left plot of Fig. 14 and in the two plots of Fig. 15, the rendering of the free surface is also presented. Remarkably, while with this single-phase model the underwater vortical structures are, as already mentioned, rather similar to what was drawn by da Vinci, the water pool surface remains almost flat and smooth and thus very far from that drawn by Leonardo, on the contrary. This is the subject of Sec. VI D.

D. Air–water simulations

From Sec. VI C, it is clear that modeling the liquid phase alone is not enough to reproduce the flow drawn in the sheet RCIN 912660. In order to get closer to Leonardo's drawing, the air phase was added in the numerical model. As a first attempt, the air phase was introduced in the domain as dispersed in the water jet: following the work by

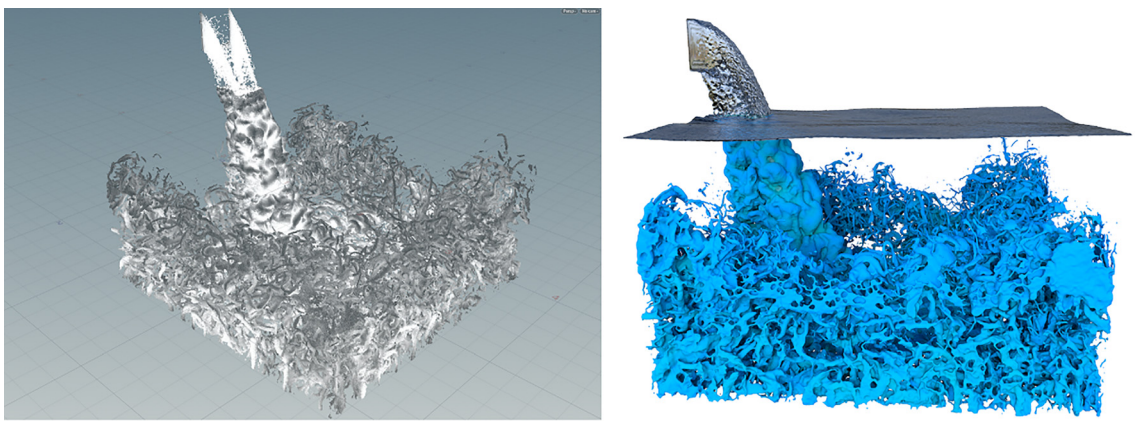

FIG. 14. SPH simulation using a single-phase model (air phase is not included)—final configuration. Left: subset of the particles having $|\boldsymbol{\omega}| < 30\ \mathrm{s}^{-1}$. Right: rendering of the iso-surface of the modulus of the vorticity field $|\boldsymbol{\omega}| = 30\ \mathrm{s}^{-1}$. Time instant 5.0 s.

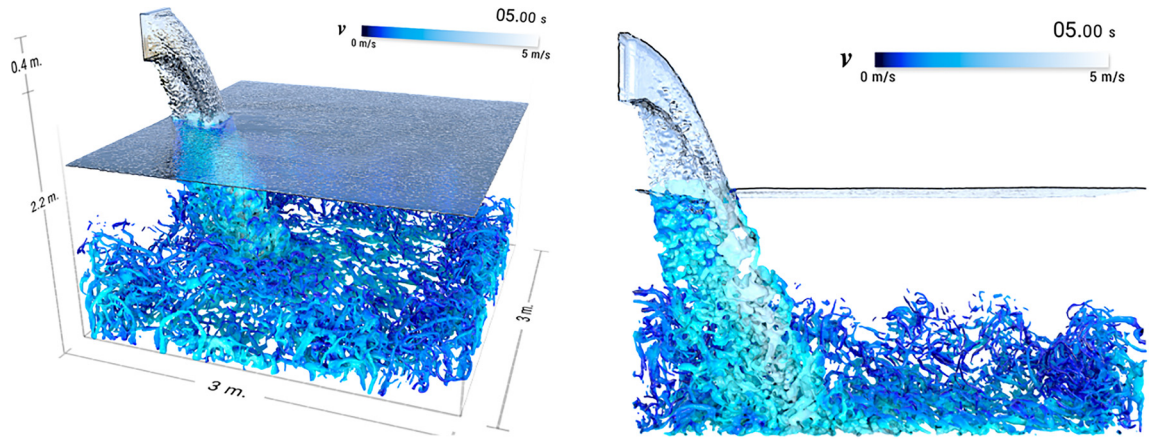

FIG. 15. SPH simulation using a single-phase model (air phase is not included)—final configuration. Rendering of the iso-surface $Q = 200\ s^{-2}$ and of the free surface. The iso-surface is colored with the intensity of the velocity field. Left: 3D view with the main lengths. Right: lateral view using half fluid domain.

Chanson *et al.*,[6] a percentage of 20% of air inside the jet was used, which corresponds to a characteristic value of high air content in a supercritical channel flow. Hence, the air particles were positioned randomly in the inflow with a ratio 1:5 to the liquid particles.

However, as is well known in the literature (see, e.g., Refs. 31 and 34), the air entrapped in the shear layer during the jet penetration plays an important role too. This can be achieved by modeling the whole air domain with air particles. However, this would imply a significant increase in CPU costs associated with the substantial increase in total particle number. In order to avoid this but to still account as much as possible for the surrounding air presence, in the inlet flow a frame of air particles was added surrounding the square section from which the water jet originated, see Fig. 16. The thickness of the air frame is equal to 0.027 m, corresponding to $4\Delta r$. In this way, part of the air plunges in the water, entrapped in the shear layer generated by the jet. This partial filling of the air domain is possible within the SPH model thanks to the equation of state, given by Eq. (1), used. Indeed, the air particles are surrounded by a free surface, i.e., a constant pressure acts on the modeled air domain surface and therefore the air particles are confined and do not wander from the jet. Because of the complexities related to the use of air frame surrounding the water jet, in this configuration a uniform inlet velocity was enforced for both air and water particles.

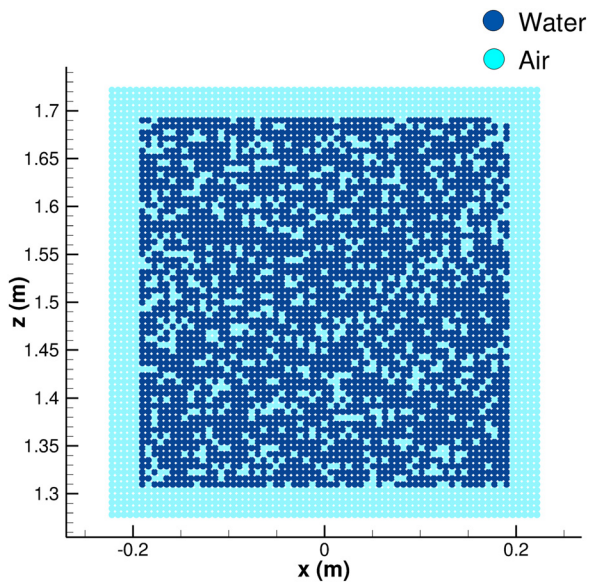

FIG. 16. SPH simulation using an air–water model: layout of the fluid particle phases generated at the inlet plane.

In the left plot of Fig. 17, an iso-Q surface of the flow is depicted at $t = 2.6$ s. The air bubbles entrapped in the jet flow detach from the main current and rise toward the free surface. In their motion, they generate vorticity associated with the boundary layer at their air–water interface, thus generating a perturbation along the main jet current. When they finally reach the free-surface, they burst, generating large disturbance and spray. It is also worth noting the complex toroidal vortex that is generated when the jet encounters the bottom of the tank. This can be seen better in Fig. 18 where two other views of the same time instant are shown. The annular vortex expands, keeping an almost circular shape while further transverse vortices are formed running around the main vortex tube.

In the right plot of Fig. 17, the contour plot of the velocity modulus for the air–water simulation is reported. Comparing this picture to its single-phase counterpart in Fig. 13, it can be noticed that in the two-phase simulation some turbulent structures detach in the bubbly fluid region in front of the jet.

In Fig. 19, only the air particles are represented for two different time instants and from two different points of view: in the left plot the whole field is depicted at $t = 4.2$ s whereas in the right plot a close view below the free surface in front of the jet is shown at $t = 8.4$ s. From these views, three different regions of the flow can be recognized as follows:

(i) the jet flow in which the air is dispersed and starts aggregating in the form of small bubbles;
(ii) the liquid region in front of the jet flow where larger bubbles are formed and rise toward the free surface interacting with each other; and

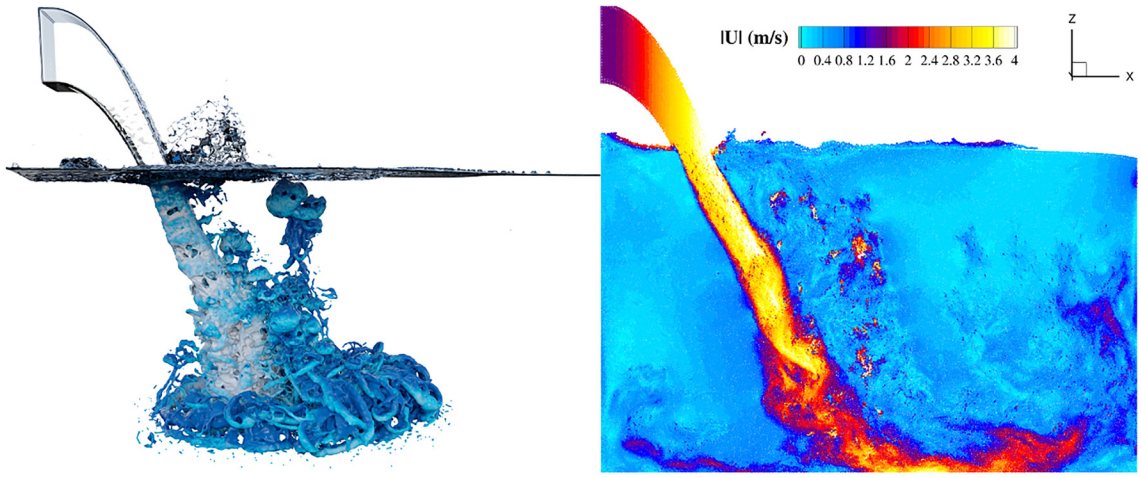

FIG. 17. SPH simulation using an air–water model—final configuration. Left: lateral view of the rendering of the iso-surface $Q = 200\ s^{-2}$ at time instant 2.6 s. The iso-surface is colored with the intensity of the velocity field. Right: mid *z*–*x* plane colored with the modulus of the velocity at time instant 5.0 s.

(iii) the area on the free surface in front of the jet where the bubbles eventually burst, creating "rosettes," similar to what was drawn by Leonardo.

In the left plot of Fig. 20, a non-photorealistic rendering of the simulation using the same colors as in Leonardo's drawing is presented. This plot highlights the air–water interaction on the pool surface. The previously mentioned "rosette" shapes due to bursting of the biggest air bubbles are clearly visible, thus reproducing one of the main flow features stressed by Leonardo in his RCIN 912660 drawing. The right plot of Fig. 20 depicts some particle trajectories from the inflow section up to their ascent to the pool surface. These curved trajectories are another flow feature stressed in Leonardo's drawing.

Finally, Fig. 21 shows the rendering of the iso-surface $Q = 200\ s^{-2}$ at time instant 5.0 s. From the left plot, it is possible to see the complex turbulent structures that are spread on the whole bottom surface and start to rise upward along the vertical walls. From the right plot, which depicts a lateral view of the half-domain, one can observe the vortices generated by the ascendant bubbly flow. This two-phase simulation involved 50 million particles on average and ran on 720 cores for about 107 h to simulate 128 000 time steps, corresponding to a physical time of 8.4 s. As supplementary material, a collection of movies related to both single- and two-phase simulations is available at the URL: https://youtu.be/zHPxK475e0w.

When looking at the post-processing of the present simulations and comparing them with the RCIN 912660 drawing, what is still missing are the large rounded curves/trajectories drawn by Leonardo on the pool surface. Our hypothesis is that these curves are mainly linked to domain confinement and since in our simulation the flow exits from the lateral and the front sides of the domain, this recirculation is not present. Furthermore, this recirculating motion of the flow around the pool would have a characteristic timescale much longer than the few seconds computed in our simulation. This topic deserves further investigation and leaves the door open to further studies of the RCIN 912660 drawing.

VII. CONCLUSION

Five hundred years after the death of Leonardo Da Vinci in Amboise, a French-Italian research team has tried to reproduce the

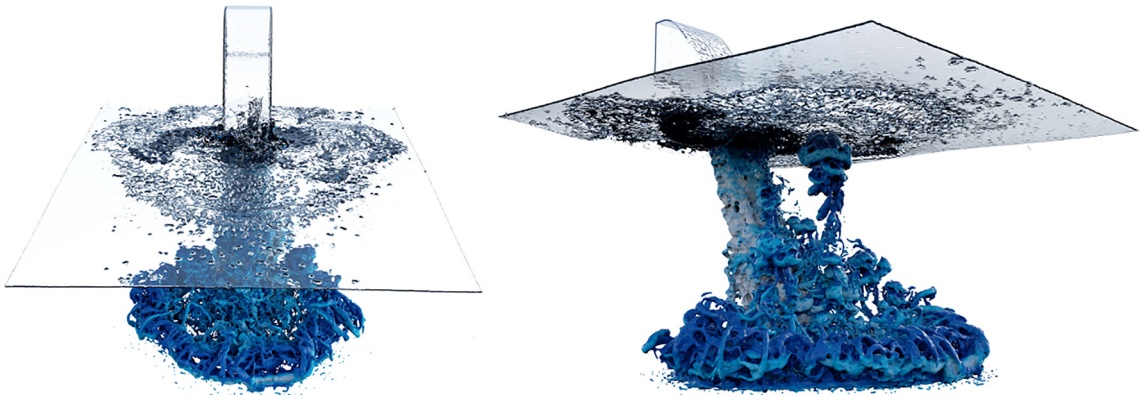

FIG. 18. SPH simulation using an air–water model—final configuration. Rendering of the iso-surface $Q = 200\ s^{-2}$ at time 2.6 s. The iso-surface is colored with the intensity of the velocity field.

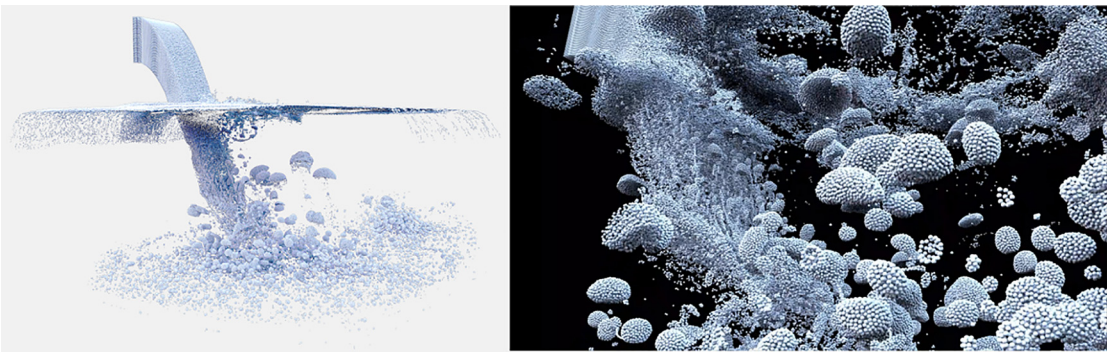

FIG. 19. SPH simulation using an air–water model—final configuration. Rendering of the air particles. Left: side view at time instant 4.2 s. Right: bottom view at time instant 8.4 s.

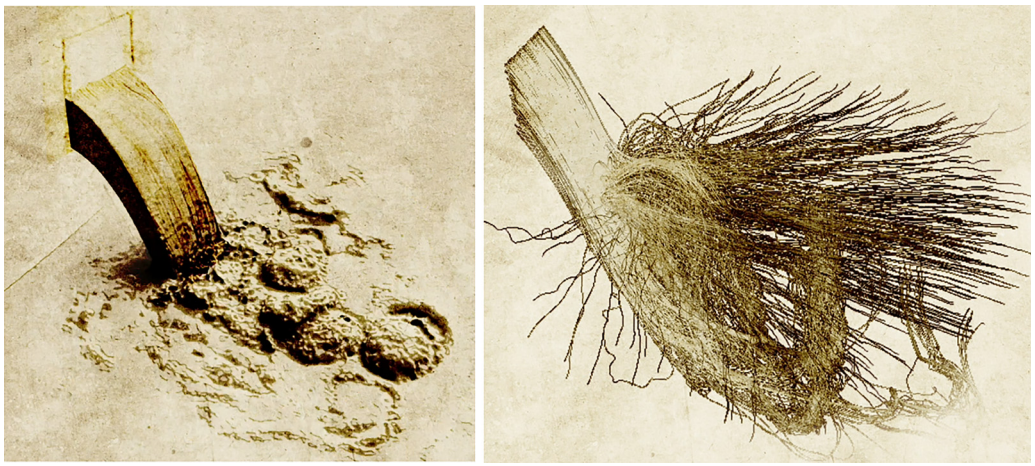

FIG. 20. SPH simulation using an air–water model—final configuration. Left: non-photorealistic rendering, top view at time instant 5.8 s. Right: trajectories of water particles from the inflow up to their ascent to the pool surface.

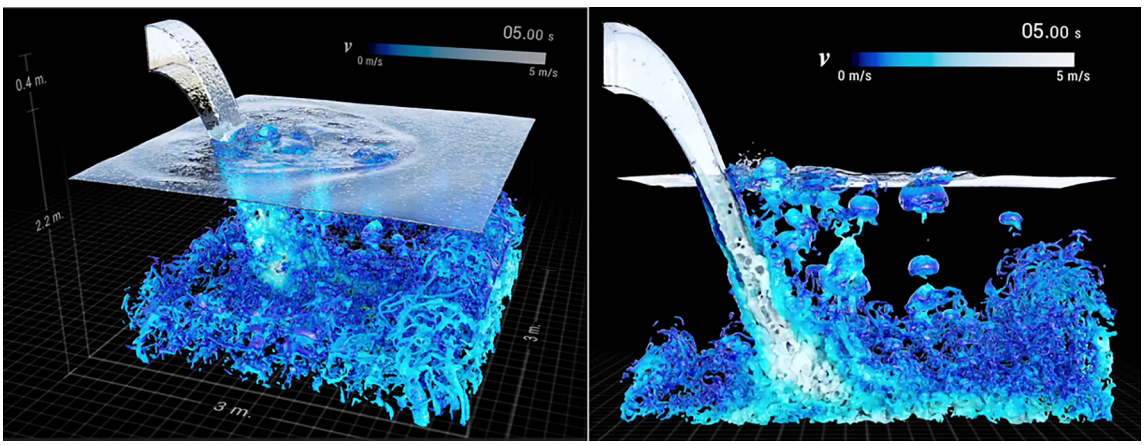

FIG. 21. SPH simulation using an air–water model—final configuration. Rendering of the iso-surface $Q = 200\ s^{-2}$ at time 5.0 s. The iso-surface is colored with the intensity of the velocity field.

physics behind one of his most famous and elaborate drawings of water studies. Leonardo Da Vinci was a fine observer of water flows. He was able to extract essential phenomena of complex air–water flows and accurately describe each flow feature independently from the others, both in his drawings and in their accompanying notes. The complexities of the flow features highlighted by Leonardo are linked to the vortical structures generated by an air–water flow in which air entrainment plays a significant role. These conditions made the numerical simulation of his drawing very challenging.

To tackle this problem, the SPH numerical method was selected and its further extension to turbulent flows, called δ-LES-SPH, was adopted and adapted to multi-phase flows by the team.

Initial difficulties arose from the lack of knowledge of the flow conditions observed by Leonardo. Successive hypotheses were made on the geometry and inflow and outflow. Three-dimensional numerical simulations were performed on a supercomputer using tens of millions of fluid elements. A sophisticated graphical rendering was needed to visualize the large amount of data. Initial results showed that the role of the air entrained by the water jet is crucial in driving turbulent structures at the surface in front of the jet. In the end, in the final simulation run, one can recognize very similar features to the ones in the drawing by Leonardo, but much more detailed of course, and the analysis is still in progress.

ACKNOWLEDGMENTS

The present work was funded by Ecole Centrale Nantes, which provided technical and IT support. For this support, the authors would like to thank Nicolas Moës (ECN, Professor, Dean for research, Member of the Académie des Sciences); Luisa da Silva (ECN, Researcher, Head of the ICI supercomputing center); Patrick Roustang and Romain Plourde (ECN, Audiovisual technicians); and Sandrine Jamet (ECN, Public relations manager of LHEEA Lab).

The SPH simulations performed under the present research were obtained using the SPH-Flow solver, software developed within a collaborative consortium composed of Ecole Centrale Nantes, NextFlow Software company and CNR-INM. The authors would like to thank Guillaume Oger (ECN, Researcher, High Performance Computing and numerical methods) and Matthieu De Leffe (NextFlow Software, Head of solvers development) for the software help and support.

For the support received on the study of Leonardo's works, the authors are grateful to Jean Dhombres [Centre Alexandre Koyré (EHESS/CNRS), Historian of Science]; Rodolfo Papa (Accademia Urbana Delle Arti, Historian of Art); Flavia Polignano (Rome, Historian of Art); and Michele Di Monte (Gallerie Nazionali d'Arte Antica di Roma—Palazzo Barberini-Galleria Corsini, Historian of Art, Faculty Member).

For the support received from the CNR-INM, the authors would like to thank Matteo Antuono, Danilo Durante, and Mario Felli (CNR-INM, Researchers) and Massimo Guerra (CNR-INM, Audiovisual technician).

Finally, the authors acknowledge the support provided by the Museo Leonardiano (Vinci, Tuscany); Dr. Mario Bernardi (Villa Basilica, Physicist); and Michele Lurci (Villa Basilica, former Deputy mayor and councilor for culture).

The research activity was developed within the Project Area Applied Mathematics of the Department of Engineering, ICT and Technology for Energy and Transport (DIITET) of the Italian National Research Council (CNR).

AUTHOR DECLARATIONS

Conflict of Interest

The authors have no conflicts to disclose.

DATA AVAILABILITY

The data that support the findings of this study are available from the corresponding author upon reasonable request.

REFERENCES

[1]R. J. Adrian, "Particle-imaging techniques for experimental fluid mechanics," Annu. Rev. Fluid Mech. **23**(1), 261–304 (1991).
[2]M. Antuono, A. Colagrossi, and S. Marrone, "Numerical diffusive terms in weakly-compressible SPH schemes," Comput. Phys. Commun. **183**(12), 2570–2580 (2012).
[3]M. Antuono, S. Marrone, A. D. Mascio, and A. Colagrossi, "Smoothed particle hydrodynamics method from a large eddy simulation perspective," Phys. Fluids **33**(1), 015102 (2021).
[4]M. Antuono, P. N. Sun, S. Marrone, and A. Colagrossi, "The δ-ALE-SPH model: An arbitrary Lagrangian-Eulerian framework for the δ-SPH model with particle shifting technique," Comput. Fluids **216**, 104806 (2021).
[5]C. Brücker, "3-D measurements of bubble motion and wake structure in two-phase flows using 3-D scanning particle-image-velocimetry (3-D SPIV) and stereo-imaging," in *Laser Techniques Applied to Fluid Mechanics* (Springer, 2000), pp. 621–635.
[6]H. Chanson, "Measuring air-water interface area in supercritical open channel flow," Water Res. **31**(6), 1414–1420 (1997).
[7]M. Clayton, *Leonardo Da Vinci: A Life in Drawing* (Royal Collection Trust, 2018).
[8]A. Colagrossi and M. Landrini, "Numerical simulation of interfacial flows by smoothed particle hydrodynamics," J. Comput. Phys. **191**(2), 448–475 (2003).
[9]G. B. Deane, M. D. Stokes, and A. H. Callaghan, "Turbulence in breaking waves," Phys. Today **69**(10), 86 (2016).
[10]G. B. Deane, M. D. Stokes, and M. I. Latz, "Bubble stimulation efficiency of dinoflagellate bioluminescence," Luminescence **31**(1), 270–280 (2016).
[11]A. D. Mascio, M. Antuono, A. Colagrossi, and S. Marrone, "Smoothed particle hydrodynamics method from a large eddy simulation perspective," Phys. Fluids **29**(3), 035102 (2017).
[12]A. Donnithorne, *Leonardo Da Vinci: A Closer Look* (Royal Collection Trust, 2019).
[13]L. E. Drain, *The Laser Doppler Techniques* (Chichester, 1980).
[14]R. Ecke, "The turbulence problem: An experimentalist's perspective," Los Alamos Sci. **29**, 124–141 (2005).
[15]M. Felli, "Underlying mechanisms of propeller wake interaction with a wing," J. Fluid Mech. **908**, A10 (2021).
[16]M. Felli and M. Falchi, "Propeller wake evolution mechanisms in oblique flow conditions," J. Fluid Mech. **845**, 520 (2018).
[17]R. A. Gingold and J. J. Monaghan, "Smoothed particle hydrodynamics: Theory and application to non-spherical stars," Mon. Not. R. Astron. Soc. **181**(3), 375–389 (1977).
[18]N. Grenier, M. Antuono, A. Colagrossi, D. Le Touzé, and B. Alessandrini, "An Hamiltonian interface SPH formulation for multi-fluid and free surface flows," J. Comput. Phys. **228**(22), 8380–8393 (2009).
[19]I. Hammani, S. Marrone, A. Colagrossi, G. Oger, and D. Le Touzé, "Detailed study on the extension of the δ-SPH model to multi-phase flow," Comput. Methods Appl. Mech. Eng. **368**, 113189 (2020).
[20]D. Jackson and B. Launder, "Osborne Reynolds and the publication of his papers on turbulent flow," Annu. Rev. Fluid Mech. **39**, 19–35 (2007).
[21]A. N. Kolmogorov, "Equations of turbulent motion in an incompressible fluid," Dokl. Akad. Nauk SSSR **30**, 299–303 (1941).

[22]L. B. Lucy, "A numerical approach to the testing of the fission hypothesis," Astron. J. **82**, 1013–1024 (1977).
[23]E. O. Macagno, *Leonardian Fluid Mechanics in the Codex Atlanticus: General Survey*, IIHR Monograph Series 100 (University of Iowa, 1986).
[24]E. O. Macagno, *Leonardian Fluid Mechanics: 'Libro dell'acqua' IV*, IIHR Monograph Series 122 (University of Iowa, 2002).
[25]S. Marrone, A. Colagrossi, D. Le Touzé, and G. Graziani, "Fast free-surface detection and level-set function definition in SPH solvers," J. Comput. Phys. **229**(10), 3652–3663 (2010).
[26]I. Marusic and S. Broomhall, "Leonardo da Vinci and fluid mechanics," Annu. Rev. Fluid Mech. **53**, 1–25 (2021).
[27]J. J. Monaghan, "Simulating free surface flows with SPH," J. Comput. Phys. **110**(2), 399–406 (1994).
[28]J. J. Monaghan, "SPH without a tensile instability," J. Comput. Phys. **159**(2), 290–311 (2000).
[29]J. J. Monaghan and J. B. Kajtar, "Leonardo da Vinci's turbulent tank in two dimensions," Eur. J. Mech.-B/Fluids **44**, 1–9 (2014).
[30]S. Nugent and H. A. Posch, "Liquid drops and surface tension with smoothed particle applied mechanics," Phys. Rev. E **62**(4), 4968 (2000).
[31]C. D. Ohl, H. N. Oguz, and A. Prosperetti, "Mechanism of air entrainment by a disturbed liquid jet," Phys. Fluids **12**(7), 1710–1714 (2000).
[32]R. Papa, *La "Scienza Della Pittura" di Leonardo: Analisi Del "Libro di Pittura"* (Medusa Edizioni, 2005).
[33]S. B. Pope, "Ten questions concerning the large-eddy simulation of turbulent flows," New J. Phys. **6**(1), 35 (2004).
[34]A. Prosperetti and H. N. Oguz, "Air entrainment upon liquid impact," Philos. Trans. R. Soc. London. Ser. A **355**(1724), 491–506 (1997).
[35]P. W. Randles and L. D. Libersky, "Smoothed particle hydrodynamics: Some recent improvements and applications," Comput. Methods Appl. Mech. Eng. **139**(1–4), 375–408 (1996).
[36]O. Reynolds, "XXIX. An experimental investigation of the circumstances which determine whether the motion of water shall be direct or sinuous, and of the law of resistance in parallel channels," Philos. Trans. R. Soc. London **174**, 935–982 (1883).
[37]J. Schaye, R. A. Crain, R. G. Bower, M. Furlong, M. Schaller, T. Theuns, C. Dalla Vecchia, C. S. Frenk, I. G. McCarthy, J. C. Helly *et al.*, "The eagle project: Simulating the evolution and assembly of galaxies and their environments," Mon. Not. R. Astron. Soc. **446**(1), 521–554 (2015).
[38]C. Shen, J. F. O'Brien, and J. R. Shewchuk, "Interpolating and approximating implicit surfaces from polygon soup," in *ACM SIGGRAPH 2004 Papers, SIGGRAPH '04* (Association for Computing Machinery, New York, 2004), pp. 896–904.
[39]J. Smagorinsky, "General circulation experiments with the primitive equations: I. the basic experiment," Mon. Weather Rev. **91**(3), 99–164 (1963).
[40]M. D. Stokes, G. B. Deane, M. I. Latz, and J. Rohr, "Bioluminescence imaging of wave-induced turbulence," J. Geophys. Res.: Oceans **109**(C1), C01004, https://doi.org/10.1029/2003JC001871 (2004).
[41]P. N. Sun, A. Colagrossi, S. Marrone, M. Antuono, and A. M. Zhang, "Multi-resolution δ-plus-SPH with tensile instability control: Towards high Reynolds number flows," Comput. Phys. Commun. **224**, 63–80 (2018).
[42]P. N. Sun, A. Colagrossi, S. Marrone, M. Antuono, and A. M. Zhang, "A consistent approach to particle shifting in the δ-plus-SPH model," Comput. Methods Appl. Mech. Eng. **348**, 912–934 (2019).
[43]P. N. Sun, A. Colagrossi, S. Marrone, and A. M. Zhang, "Detection of Lagrangian coherent structures in the SPH framework," Comput. Methods Appl. Mech. Eng. **305**, 849–868 (2016).
[44]J. W. Swegle, D. L. Hicks, and S. W. Attaway, "Smoothed particle hydrodynamics stability analysis," J. Comput. Phys. **116**, 123–134 (1995).
[45]K. Szewc, J. Pozorski, and J. P. Minier, "Spurious interface fragmentation in multiphase SPH," Int. J. Numer. Methods Eng. **103**(9), 625–649 (2015).
[46]H. Tennekes and J. L. Lumley, *A First Course in Turbulence* (MIT Press, 2018).